Background $E \times B$ shear nonlinear gyrokinetic benchmark

F.J. Casson

February 23, 2011

Abstract

This draft thesis extract contains a study of resolution and dissipation issues for the $E \times B$ shear method implemented in GKW and GS2. It expands on the benchmark between GKW and GYRO in [F.J. Casson et al. Physics of Plasmas, **16**, 092303 (2009) [1]], exploring some issues regarding resolution and dissipation that should be considered when dealing with strong $E \times B$ shearing, in particular for the case of self-sustained turbulence. It is circulated with the intention of stimulating discussion and gauging enthusiasm for a more comprehensive and collaborative nonlinear benchmark of $E \times B$ shearing between the codes, which would be more suitable for publication. If this document needs to be cited, please cite my forthcoming PhD Thesis, Uni. Warwick, 2011.

1 Initial benchmark

The implementation of background $E \times B$ shearing in both GKW and GS2 is the one first suggested by Hammett [2], in which the distribution function is discretely remapped between radial wavenumbers. Further details of the implementation in GKW are given in Ref. [3].

Previous work with both gyrofluid and gyrokinetic codes has quantified the quenching effect of background $E \times B$ shear on tokamak turbulence and established the phenomenological relation for the turbulent diffusivity

$$\chi_i = \chi_{i0}(1 - \alpha_E \gamma_E / \gamma_{\max}), \qquad (1)$$

where α_E is a constant of order unity, and $\gamma_{\max}$ is the maximum linear growth rate of the system in the absence of the sheared flow. The initial gyrofluid results [4–6] found $\alpha_E \sim 1$, and later gyrokinetic results found $\alpha_E \sim 0.5$ [1, 7–9].[1]

In this section we present a benchmark of the GKW implementation of $E \times B$ shearing against the results of Ref. [9] using the GYRO code [10]. The implementation in GYRO makes use of finite differences in the radial direction, with damped boundary regions allowing for a direct implementation of a non-periodic shear flow in a local domain [8]. Since this method differs significantly from that used in GKW, a benchmark is of interest. Our implementation has also been benchmarked against the GS2 code [11] for the Cyclone case results presented in Ref. [12], with good agreement. Since the numerical implementation of the shearing in both codes is identical, it is of less interest to present this benchmark here.

The benchmark is for the collisionless Waltz standard case [4, 5, 13] of a deuterium plasma with $R/L_T = 9$, $R/L_N = 3$, electron to ion temperature ratio $T_e/T_i = 1$, mass ratio $\sqrt{(m_i/m_e)} = 60$, safety factor $q = 2$, magnetic shear $\hat{s} = 1$, and inverse aspect ratio $\epsilon = r/R = 0.16$. This case is referred to throughout this thesis as the GA-STD case. Results are presented in the standard gyro-Bohm units where a is the plasma minor radius with $R/a = 3$, $c_s = \sqrt{T_e/m_i}$ is the ion sound speed, $\rho_s = c_s/\Omega_{ci}$ is the ion-sound Larmor radius, and $\Omega_{ci} = eB/m_i$ is the ion cyclotron frequency evaluated on the magnetic axis.

Both codes are run in the local limit with the model '$s-\alpha$' equilibrium with the MHD parameter $\alpha = 0$. In this geometry, the shearing rate for both

[1] It appears that the elimination of the boundary discontinuity altered the result from $\alpha_E = 1.18$ in Ref. [4] to $\alpha_E = 0.69$ in Ref. [6], thus some of the difference may not be between gyrofluid and gyrokinetic, but due to the boundary conditions.

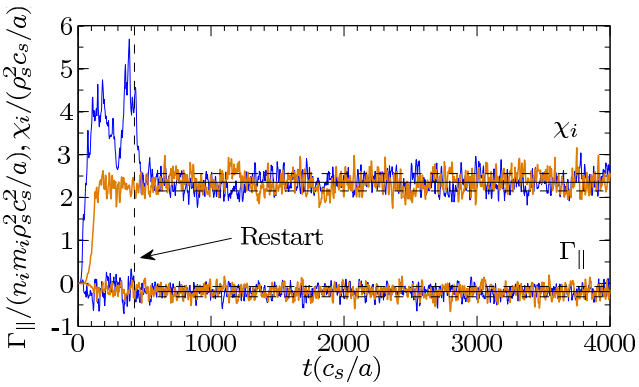

Figure 1: Time traces of ion heat diffusivity and momentum flux for the restart method (blue, thin) compared to a run without restart (orange, thick) with $\gamma_E = 0.118(c_s/a)$ with means and variances $\bar{\chi}_i = (2.354 \pm 0.202, 2.353 \pm 0.218)$ and $\bar{\Gamma}_\parallel = (-0.191 \pm 0.119, -0.188 \pm 0.127)$ for the restart and non-restart methods respectively.

codes is equivalent to the familiar definition [14, 15]:

$$\gamma_E \approx \frac{(RB_p)^2}{B_t}\frac{\partial^2 \Phi}{\partial \Psi^2} \approx \frac{dv_E}{dr}, \qquad (2)$$

where Ψ is the poloidal flux. The values of the maximum linear growth rate $\gamma_{\max}$ and other linear properties for the simulations of this case are given in Table 1 and results in this section are presented in terms of $\gamma_E/\gamma_{\max}$.

Table 1: Most unstable linear modes: Growth rate $\gamma_{\max}$, with corresponding mode frequency ω and scale $k_\theta \rho_s$. Positive values of ω indicate propagation in the ion diamagnetic direction.

$\hat{s}$	$\gamma_{\max}(a/c_s)$	$\omega(a/c_s)$	$k_\theta \rho_s$
Adiabatic electrons			
-0.50	0.119	0.272	0.44
1.00	0.132	0.296	0.31
Kinetic electrons			
1.00	0.265	0.324	0.28

In simulations with a high $E \times B$ shear rate, the linear growth can be suppressed such that the simulation takes an impractically long time to reach the nonlinear saturated state, or in some cases never will. However, if the simulation is initialised without background $E \times B$ shear, and the shear is applied once the nonlinear phase is reached, then the system will quickly reach a new saturated state. In the case where linear growth in completely suppressed, this state is referred to as 'subcritical' or 'self-sustained' turbulence [16–18], and has been conjectured to play a role in transport bifurcations leading to transport barriers [5, 19]. If the turbulence is not in this state (i.e linearly unstable with $E \times B$ shear), we find that the statistical properties of the saturated nonlinear state are unaffected by the path taken to get there (Fig. 1). All results presented here are obtained with the restart method for larger γ_E , and all time averages are taken over a minimum range of $t_{av} = 1600(a/c_s)$ after the new saturated state was reached, unless otherwise specified.

Unless otherwise stated, all simulations with adiabatic electrons are performed with $N_{\text{mod}} = 16$ binormal modes and $N_x = 83$ radial modes. The maximum wavevector has binormal wavenumber $k_\theta \rho_s = 0.75$ where k_θ is evaluated at the outboard midplane and ρ_s is evaluated at the magnetic axis. The mode spacing gives a perpendicular simulation domain of extent $[L_{\text{radial}}, L_{\text{binormal}}] = [120, 126]\rho_s$. The number of grid points in parallel velocity, magnetic moment, and along the field line are $N_{v\parallel} = 16$, $N_\mu = 8$ and $N_s = 16$ respectively. These grid sizes have proved sufficient to investigate the physics phenomena. The adiabatic results (away from the critical shear region) are well converged in N_s, N_μ and N_x, and $N_{v\parallel}$, and to within 10% in N_{mod} (increasing L_{binormal}).

All simulations with kinetic electrons are performed with $N_{\text{mod}} = 21$ binormal modes with a maximum $k_\theta \rho_s = 1.0$, and $N_x = 167$ radial modes with a perpendicular simulation domain of

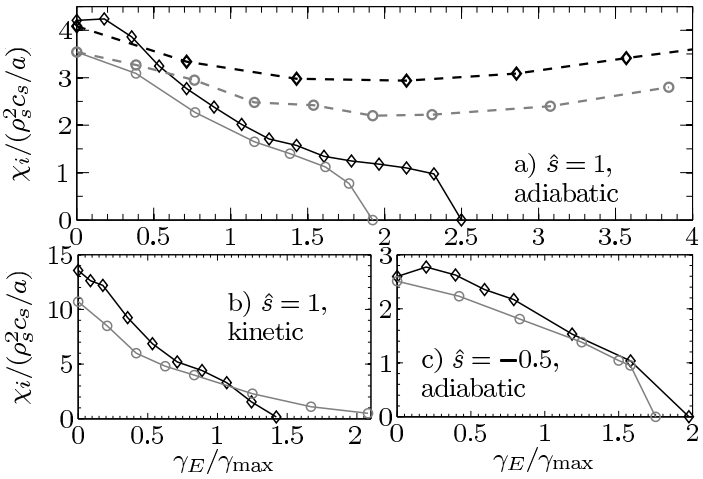

Figure 2: GKW benchmark of background $E \times B$ shear with GYRO for the GA-STD case. GKW results (diamonds) for a) adiabatic electrons, b) kinetic electrons, and c) adiabatic with $\hat{s} = -0.5$, are compared to the equivalent GYRO results (circles) from Tables II, III, IV and V of Ref. [9]. The dashed lines in a) include coupled parallel velocity shear for purely toroidal rotation with $u' = 12\gamma_E$. Standard dissipation, $[\alpha_x, \alpha_s, \alpha_{vp}] = [0.0, 1.8, 1.8]$.

extent $[L_{\text{radial}}, L_{\text{binormal}}] = [120, 126]\rho_s$. The number of points in the parallel velocity is increased to $N_{v\parallel} = 32$ as compared with the adiabatic case. The kinetic results are well converged in N_s, N_μ and N_x, and to within 20% in N_{mod} (increasing L_{binormal}) and $N_{v\parallel}$. These convergences are for cases without strong shear, convergence in the critical shear region is examined in the next section. Except where stated otherwise, all results presented in this section are for adiabatic electrons.

The resolution used in the GKW simulations is chosen to be comparable to the gridsizes used in Ref. [9] (though it should be noted that the numerics of the codes are different). In particular, both sets of results were obtained with $N_{\text{mod}} = 16$ binormal modes over the same range of wavenumbers.

The correspondence between the linear growth rates predicted by GKW (Table 1) and GYRO (Ref. [9], Table I) is nearly exact. The comparison between the two codes for the nonlinear turbulent ion diffusivity quenching with shearing is shown in Fig. 2, and the GKW results are given in tablular form in Ref. [1]. As is standard, for these simulations (and those in Chapter 5), GKW was run with no hyper-dissipation perpendicular to the field, and a small amount of hyper-dissipation in the finite difference directions (s and $v_\parallel$) which stabilises the numerics ($\alpha_s = 1.8, \alpha_{vp} = 1.8$). Both the GKW and GYRO simulations are collisionless, and both codes use the restart method to access the self-sustained turbulence region.

It can be seen that GKW ion heat diffusivities are up to 25% higher, and that there is some disagreement between the codes in the critical shear region where the turbulence becomes completely suppressed. These differences are investigated in more detail in the next section. Notwithstanding the above, GKW and GYRO give good agreement for the turbulence quench relation (Eq. (1)) with close concurrence on the important parameter $\alpha_E \approx 0.4-0.6$ (depending on the case) which quantifies the strength of the shear suppression. This agreement gives good confidence in the qualitative physics predicted by both codes.

For adiabatic electrons, the benchmark was also conducted including the destabilising effect of parallel velocity shear $u' = 12\gamma_E$ consistently for purely toroidal rotation, also shown in Fig. 2. Here too the codes give good agreement, both predicting a minimum in the heat transport at $\gamma_E = 2\gamma_{\max}$.

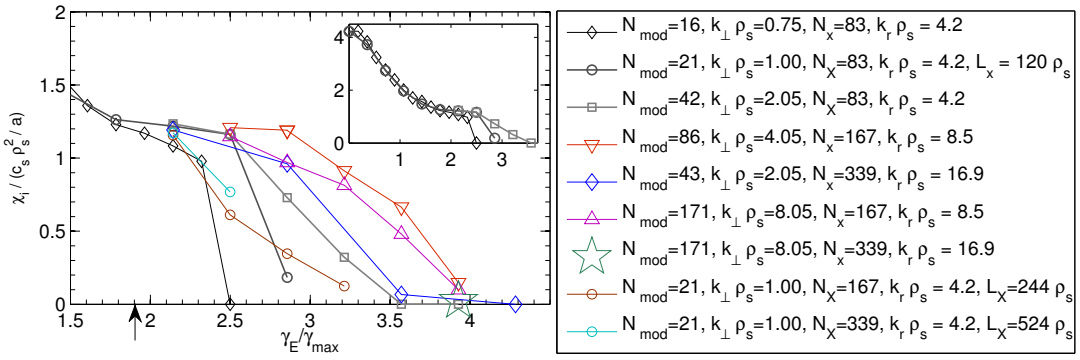

Figure 3: GKW results investigating the effect of increased perpendicular resolution in the critical shear region (without collisions or perpendicular dissipation). Time averages are over at least $t_{av} = 300(a/c_s)$, due to expensive nature of these computations and the low variance for these points. Standard dissipation, $[\alpha_x, \alpha_s, \alpha_{vp}] = [0.0, 1.8, 1.8]$. Here $k_\perp$ refers to maximum k_θ.

2 Effect of resolution and dissipation

As was noted in Ref. [9], the region near the critical shear is difficult to resolve properly, indeed this is the region in which the two codes show worst agreement. A convergence study in $N_{\rm mod}$ and N_x in the critical shear region for the adiabatic case was undertaken with GKW. Simulations conducted with higher perpendicular resolution ($k_\theta \rho_s$ up to 8.05 and $k_\psi \rho_s$ up to 16.9) indicate that the region near the critical shear is sensitive to this resolution, with a longer 'tail' in the residual turbulent flux at high shear rates ($\gamma_E/\gamma_{\rm max} > 2$), as compared with the lower resolution results (Fig. 3). This is not surprising since the effect of the $E\times B$ shear is to break up structures, pushing the turbulence to smaller scales. The results initially indicate that this tail is 'converged' when the maximum resolved scales are $k_\theta \rho_s = 4.05$ and $k_\psi \rho_s = 4.2$ and higher, but as we show later, this convergence does not mean the result is physical. Whilst the shearing acts to directly increase only the k_ψ scales, nonlinear mixing also results in a similar resolution requirement in the binormal direction. (For kinetic simulations containing trapped electron modes extended along the field, greater radial resolution is usually required due to the magnetic shear coupling, even in the absence of $E\times B$ shear.)

As discussed in Ref. [3], for the wavevector remapping method, convergence in radial resolution $L_{\rm radial}/L_{\rm binormal}$ should be checked; Fig. 4 demonstrates the results are well converged for the low shear cases when the remapping occurs most infrequently. For the simulations with adiabatic electrons at lower resolutions, there is a sharp transition from the self-sustained turbulent state at the high shear limit. The convergence in $L_{\rm radial}/L_{\rm binormal}$ for these points is shown in Fig. 3 and Fig. 5; increased $L_{\rm radial}$ gives a smoother end to the tail and eliminates the sharp transition, but does not move the critical point at which the turbulence is suppressed. Very close to the critical shear therefore, the discrete nature of the shearing implementation allows turbulence to persist in the time between the remapping.

To investigate further if the tail in the turbulent heat flux at high shear is physical, we attempted to improve on the benchmark between GKW and GYRO. In an effort to better understand the differences, a few test simulations were made with GYRO, concentrating on the adiabatic case with $\hat{s} = 1$.[2]

We began by trying to understand the 17% difference in diffusivity at zero $E\times B$ shear (Fig. 2). Both codes are well converged for the adiabatic results (with the slight exception of the number of binormal modes, for which $N_{\rm mod} = 16$ was used in both for the benchmark) By running GYRO in flux

[2]Thanks to W. Guttenfelder for running the GYRO simulations.

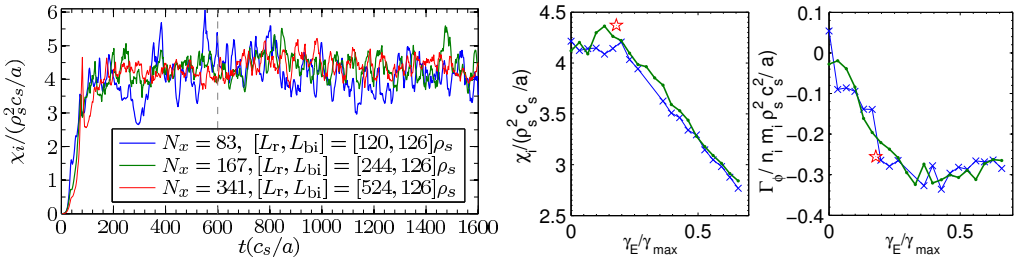

(a) $\gamma_E = 0.19\gamma_{\max}$, applied from $t = 0$.

(b) $\gamma_E = (0, 0.65)\gamma_{\max}$, same legend colours.

Figure 4: $L_{\text{radial}}/L_{\text{binormal}}$ convergence check of the $E\times B$ shearing implemented in GKW, with L_{binormal} held constant for small γ_E, when the remapping is infrequent. The averages over $t_{av} = 1000(a/c_s)$ for a) are $\bar{\chi}_i^{120}(a/c_s\rho_s^2) = 4.16 \pm 0.50$, $\bar{\chi}_i^{244}(a/c_s\rho_s^2) = 4.38 \pm 0.38$, $\bar{\chi}_i^{524}(a/c_s\rho_s^2) = 4.42 \pm 0.29$, with increasing L_{radial}. The variance decreases with increasing L_{radial} (since the average is over a larger domain) but the χ_i mean is converged to within 5% for $\gamma_E > 0.19\gamma_{\max}$. In b) the time averaged fluxes demonstrate that the results are well converged as the effect of the shear increases. The average momentum fluxes are close to zero (see Fig. 1), so their variance is relatively large.

tube mode, it was checked that the non periodic radial damped boundaries do not make any difference to the result at zero $E\times B$ shear (this cannot be checked at finite $E\times B$ shear, but convergence in L_{radial} could be checked instead). However, runs with newer GYRO did yield a result within 8% of the original GKW result (Fig. 5), (indeed a point close to this appears in Fig. 2 of Ref. [9], but not in the data table.)

As the next step to eliminate differences between the codes, we attempted to match numerical dissipation. GYRO uses a finite difference scheme in the radial and poloidal directions with a (upwinding) dissipation which is equivalent to a hyperdiffusive term $\sim \alpha_{r,\theta} k^4/k^4_{\max}$. GKW uses a similar scheme in the poloidal s direction, but the spectral radial direction is usually dissipation free, with some high k filtering through the dealiasing procedure. To try to match GYRO more closely, a spectral hyperdiffusive term $\sim \alpha_{x,y} k^4/k^4_{\max}$ was introduced into GKW. Since the velocity grids in the codes are rather different, matching velocity dissipation directly was not possible. We also attempted to match the codes by eliminating numerical dissipation and introducing a physical dissipation in the form of an ITER-like ion-ion collision rate $\nu_{ii} = 0.01(c_s/a)$.

The GKW results show that the critical shear region is also very sensitive to dissipation (Fig. 5). By including radial dissipation matched (as far as possible) to GYRO, the agreement between the codes is improved. At zero shear, and intermediate shear, exact agreement is found, but some differences remain at low shear and high shear. The GKW results indicate that radial dissipation, velocity space dissipation and collisions tend to reduce the turbulent tail, whilst parallel dissipation tends to increase it. We speculate that near the critical shear, any instability that survives is strongly localised in the parallel direction, which may cause numerical problems for the parallel dissipation. This is evidenced by a reduction in the tail for the simulations with $\alpha_s > 0$ when the parallel resolution is increased. Furthermore, the strong anisotropy of the turbulence prevents parallel (spatial or velocity) dissipation from being translated to dissipation at the smallest perpendicular scales, but the coupling of the two perpendicular scales through the nonlinear terms means that dissipation applied radially is quickly mixed into the binormal direction.

From the spectra for these simulations, we note that the increased flux in the cases with the longer tail comes from the largest scales, and that these cases actually have less flux at the smallest wavelengths (Fig. 6). Unsurprisingly, radial dissipation alters the shape of the radial (and binormal) spectra at the smallest scales, and the cases with collisions have the flattest spectra (i.e. the cleanest turbulent cascade). In the cases with strong $E\times B$ shear and parallel dissipation, a tendency for the k_ψ spectrum to get less steep at the smallest scales is

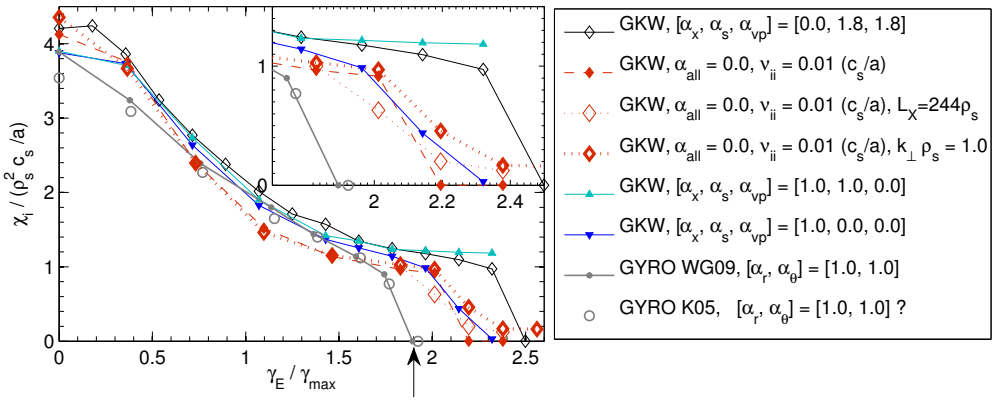

Figure 5: GKW results with varied dissipation and collisions, compared to GYRO results. K05 refers to GYRO results from Table II of Ref. [9], and WG09 refers to the same simulations repeated with a 2009 version of GYRO. For these results the original resolution (with $N_{\mathrm{mod}} = 16$) as described in Sec. 1 was used (except where indicated for the collisional runs).

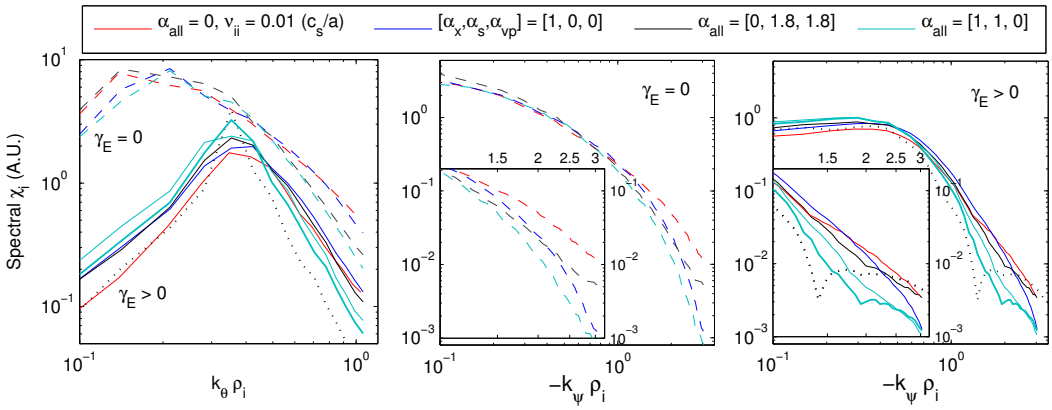

Figure 6: Spectra for the GKW results presented in Fig. 5 at zero shear (dashed), $\gamma_E/\gamma_{\max} = 1.8$ (solid), and $\gamma_E/\gamma_{\max} = 2.35$ (thick line and dotted line). The dotted line is for the case resolving up to $k_\theta \rho_s = 4.05$ and $k_\psi \rho_s = 8.5$. The k_ψ spectrum shown is the half which the turbulence is being pushed towards by the shearing. The curves plotted are the individual fluxes for each mode, and the colour scheme is the same as in Fig. 5.

amplified, and for the most extreme cases there can even be an upturn in the spectrum (corresponding to those with the longest tail in Fig. 5). This indicates a bad numerical artifact, which can cause higher overall flux at the larger scales through the inverse cascade, hence the longer tail results should be regarded as nonphysical. Note however, that these cases are not under-resolved since the cases of Fig. 3 with the highest resolution (which appear to converge) actually show this artefact most severely (Fig. 6, dotted line). The cases with collisions or radial dissipation only do not have this problem which indicates that the problem is exacerbated by parallel dissipation; when the parallel resolution is increased, the problem is mitigated and a good spectrum is obtained. This indicates that numerical problems due to strong parallel localisation can lead to incorrect results which can be identified via a coupling to the cascade.

Whilst improved agreement might be achieved by increasing the GKW radial dissipation, the ideal benchmark should focus on achieving fully con-

verged results for both codes for the case with physical collisions and minimal numerical dissipation. With this aim in mind, the GKW collisional results were also convergence tested in the critical shear region, and are well converged in N_s, L_x and maximum binormal $k_\theta \rho_s$ (Fig. 5). The collisional case has less sensitivity to the maximum $k_\theta \rho_s$ than the collisionless results of Fig. 3, and does not suffer from an (visible) numerical artefact in the radial spectrum (Fig. 6). We believe therefore that the GKW collisional results are both physical and well converged.

The first point where the turbulence remains in GKW but is completely quenched with GYRO, is at $\gamma_E/\gamma_{\max} = 1.9$. For this point, some preliminary GYRO simulations were also conducted with different box sizes and resolution, and with varied dissipation coefficients (Fig. 8). With the exception of the zero dissipation case, the GYRO results at this point all show complete turbulence quenching, even when increasing the radial box size or binormal resolution. The zero dissipation case is unphysically unstable since the GYRO entropy diagnostic [20] shows unconstrained entropy growth in the phase before the $E \times B$ shear, and both GKW and GYRO find a non stationary spreading in the k_ψ spectrum (not shown). However, we do not believe the *same* problem is occurring in the GKW simulations which show non-zero turbulence at this point, since the GKW spectra for these results are stationary (Fig. 7). Further verification of a good statistical state for the GKW results would require implementation of new diagnostics (entropy / vorticity) in GKW.[3]

It is clear that the GKW parallel dissipation α_s plays a different role to the GYRO poloidal dissipation α_θ, again probably due to the different grid implementation. Even with radial dissipation, GKW still has a tendency to predict a longer tail than GYRO, which may be explained by the difficulty of matching resolution and dissipation between codes with different numerics; in particular, the parallel velocity grid and radial numerics differ significantly between the codes.

[3]Understanding the turbulent cascade and the relationship between dissipation, energy conservation, and the steady state is currently an active and controversial area of research well beyond the scope of this thesis [18, 21, 22].

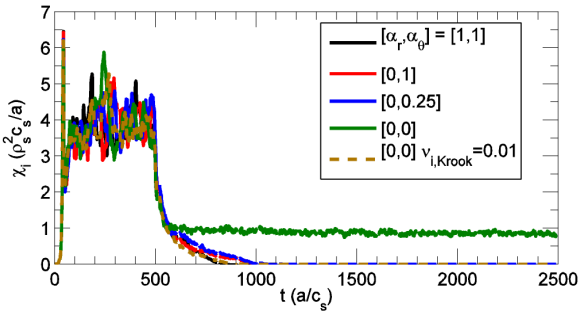

Figure 8: b) GYRO time traces for the restart method with different dissipation coefficients and collisions (dashed). The shear is $\gamma_E/\gamma_{\max} = 1.9$, corresponding to the point marked with the arrow in Fig. 5. Figure courtesy of W. Guttenfelder.

3 Summary

The benchmark is incomplete, since we have only been able to thoroughly investigate the convergence of the GKW results. However, it is expected that exact agreement could be achieved by conducting extensive convergence testing of the collisional case for both codes. We believe the remaining difference could be explained by differences in the velocity grid dissipation, the collision operator, or a minimal cascade problem in GKW. The GS2 code is more similar to GKW, differing mainly in the velocity grid, so including GS2 results in this benchmark might help to isolate where the remaining differences arise from.

To summarise, investigations with GKW have shown turbulence quenching by $E \times B$ shearing to be very sensitive to resolution and numerical dissipation in the region of the critical shear. These parameters should therefore be carefully considered when drawing conclusions in the realm of self-sustained turbulence (for example Ref. [19]). In the case of GKW, investigation of the spectral radial fluxes has revealed that the best results are obtained by minimising parallel dissipation and including either radial dissipation or collisions. When these factors are taken into account, very good (though not perfect) agreement between GKW and GYRO is found.

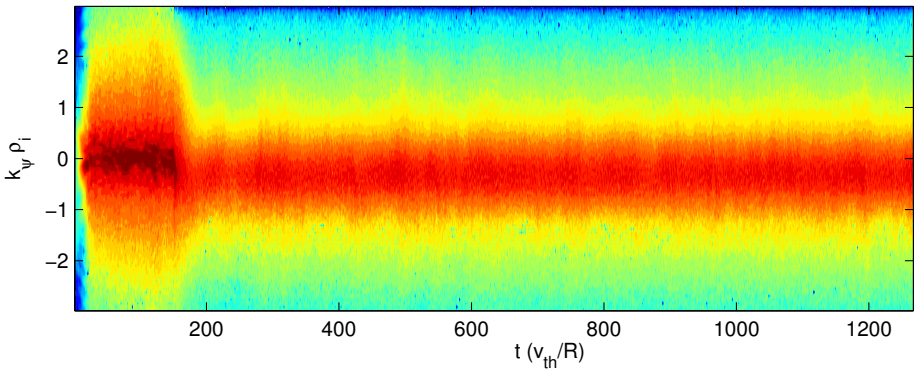

Figure 7: Time-contour plot of the χ_i spectrum (logarithmic scale, A.U.) for the collisional case in GKW with shear $\gamma_E/\gamma_{\max} = 1.8$ applied at $t = 150(R/v_{th})$.

References

[1] F. J. Casson, A. G. Peeters, Y. Camenen, et al., Phys. Plasmas **16**, 092303 (2009).

[2] G. W. Hammett, W. Dorland, N. F. Loureiro, et al., in *48th Annual Meeting of the Division of Plasma Physics, Philadelphia, (APS)* (2006), p. VP1.136.

[3] A. G. Peeters, Y. Camenen, F. J. Casson, et al., Comp. Phys. Commun. **180**, 2650 (2009).

[4] R. E. Waltz, G. D. Kerbel, and J. Milovich, Phys. Plasmas **1**, 2229 (1994).

[5] R. E. Waltz, G. D. Kerbel, J. Milovich, et al., Phys. Plasmas **2**, 2408 (1995).

[6] R. E. Waltz, R. L. Dewar, and X. Garbet, Physics of Plamas **5**, 1784 (1998).

[7] W. M. Nevins, A. M. Dimits, B. I. Cohen, et al., in *Proceedings of the Eighteenth IAEA Fusion Energy Conference, Sorrento* (2000), p. THP1/03.

[8] R. E. Waltz, J. M. Candy, and M. N. Rosenbluth, Phys. Plasmas **9**, 1938 (2002).

[9] J. E. Kinsey, R. E. Waltz, and J. Candy, Phys. Plasmas **12**, 062302 (2005).

[10] J. Candy and R. Waltz, Journal of Computational Physics **186**, 545 (2003).

[11] M. Kotschenreuther, W. Dorland, M. A. Beer, et al., Phys. Plasmas **2**, 2381 (1995).

[12] C. M. Roach, I. G. Abel, R. J. Akers, et al., Plasma Phys. Contr. F **51**, 124020 (2009).

[13] R. E. Waltz, G. M. Staebler, W. Dorland, et al., Phys. Plasmas **4**, 2482 (1997).

[14] T. S. Hahm and K. H. Burrell, Phys. Plasmas **2**, 1648 (1995).

[15] K. H. Burrell, Phys. Plasmas **4**, 1499 (1997).

[16] B. D. Scott, Physical Review Letters **65**, 3289 (1990).

[17] B. D. Scott, Physics of Fluids B: Plasma Physics **4**, 2468 (1992).

[18] B. D. Scott, Phys. Plasmas **12**, 062314 (2005).

[19] E. G. Highcock, M. Barnes, A. A. Schekochihin, et al., Physical Review Letters **105**, 215003 (2010).

[20] J. Candy and R. E. Waltz, Phys. Plasmas **13**, 032310 (2006).

[21] A. A. Schekochihin, S. C. Cowley, W. Dorland, et al., Plasma Phys. Contr. F **50**, 124024 (2008).

[22] T. Tatsuno, W. Dorland, A. A. Schekochihin, et al., Phys. Rev. Lett. **103**, 015003 (2009).